JOURNAL OF VIROLOGY, Nov. 2004, p. 12480–12488 Vol. 78, No. 22
0022-538X/04/$08.00+0 DOI: 10.1128/JVI.78.22.12480–12488.2004


# Transition from Acute to Persistent Theiler's Virus Infection Requires Active Viral Replication That Drives Proinflammatory Cytokine Expression and Chronic Demyelinating Disease†

Mark Trottier,[1,2]‡ Brian P. Schlitt,[1] Aisha Y. Kung,[1] and Howard L. Lipton[1,2,3,4]*

*Department of Neurology, Evanston Hospital, Evanston,[1] and Departments of Neurology,[3] Microbiology-Immunology and Biochemistry,[4] and Molecular Biology and Cell Biology,[2] Northwestern University, Chicago, Illinois*

Received 30 April 2004/Accepted 25 June 2004

**The dynamics of Theiler's murine encephalomyelitis virus (TMEV) RNA replication in the central nervous systems of susceptible and resistant strains of mice were examined by quantitative real-time reverse transcription-PCR and were found to correlate with host immune responses. During the acute phase of infection in both susceptible and resistant mice, levels of viral replication were high in the brain and brain stem, while levels of viral genome equivalents were 10- to 100-fold lower in the spinal cord. In the brain, viral RNA replication decreased after a peak at 5 days postinfection (p.i.), in parallel with the appearance of virus-specific antibody responses; however, by 15 days p.i., viral RNA levels began to increase in the spinal cords of susceptible mice. During the transition to and the persistent phase of infection, the numbers of viral genome equivalents in the spinal cord varied substantially for individual mice, but high levels were consistently associated with high levels of proinflammatory Th1 cytokine and chemokine mRNAs. Moreover, a large number of viral genome equivalents and high proinflammatory cytokine mRNA levels in spinal cords were only observed for susceptible SJL/J mice who developed demyelinating disease. These results suggest that TMEV persistence requires active viral replication beginning about day 11 p.i. and that active viral replication with high viral genome loads leads to increased levels of Th1 cytokines that drive disease progression in infected mice.**

*Theiler's murine encephalomyelitis virus* (TMEV) is a naturally occurring enteric pathogen of mice that belongs to the *Cardiovirus* genus in the *Picornaviridae* family (39, 41). Low-neurovirulence strains, such as BeAn and DA, produce persistent infections in the central nervous systems (CNS) of susceptible strains of mice that result in mononuclear cell inflammation and largely immune system-mediated demyelination, providing an experimental analog for multiple sclerosis (MS) in humans (6, 13, 19, 44). While only small amounts of infectious virus (100 to 1,000 PFU/spinal cord) are recovered during the persistent phase of infection (11, 29), very high levels of viral genome equivalents have been reported (49), suggesting that widespread and persistent TMEV infection involves continuous viral replication with restricted infectious virus production.

Viral antigens and RNA are largely found in neurons in the brain and spinal cord during the acute phase of infection (2, 16), whereas macrophages or microglia containing viral antigen(s) and RNA predominate in the spinal cord during chronic infection (3, 30). The spread of infection to oligodendrocytes and astrocytes is also seen (3, 9, 44, 47, 51). TMEV replication in macrophages is highly restricted at the levels of RNA replication and virion assembly, consistent with mechanisms of persistence of cytolytic RNA viruses (23, 49). The mechanism(s) underlying TMEV transition from an acute neuronal infection in the gray matter to a chronic macrophagic and glial infection in the white matter is not well understood.

One possible explanation for the difference between acute and chronic viral tropism may be the virus-specific host immune response. Ostensibly, the immune response is able to clear TMEV from the gray matter (brain and spinal cord) but not from the white matter (spinal cord) (38). Members of our laboratory previously reported very high infectious virus titers and large genome copy numbers for brains of BeAn virus-infected C.B-17 SCID mice after the acute phase of infection, in contrast to small genome copy numbers and reduced virus titers for brains of immunocompetent susceptible mice at similar time points (49). While those findings suggested the ability of host immunity to control infections in the brain, the similar levels of viral genomes found in the spinal cords of both persistently infected C.B-17 SCID and immunocompetent susceptible mice argue against the ability of the host immune response to control viral replication in that CNS tissue (49).

For the present study, we analyzed TMEV RNA replication in the brains, brain stems, and spinal cords of susceptible SJL/J and resistant C57/B6 (B6) mice by using real-time reverse transcription-PCR (RT-PCR) during the acute (days 1 to 11 postinfection [p.i.]) and transitional (days 13 to 33 p.i.) phases of CNS infection leading to viral persistence (>day 30). RT-PCR provides a large dynamic range of values and is a more sensitive measurement of TMEV persistence in the CNS than standard plaque assays. We show that the kinetics of viral RNA

* Corresponding author. Mailing address: Evanston Northwestern Healthcare Research Institute, 2650 Ridge Ave., Evanston, IL 60201. Phone: (847) 570-2168. Fax: (847) 570-1568. E-mail: hllipton@northwestern.edu.

† Supplemental material for this article may be found at http://jvi.asm.org.

‡ Present address: Biology Department, New York University, New York, NY 10003.

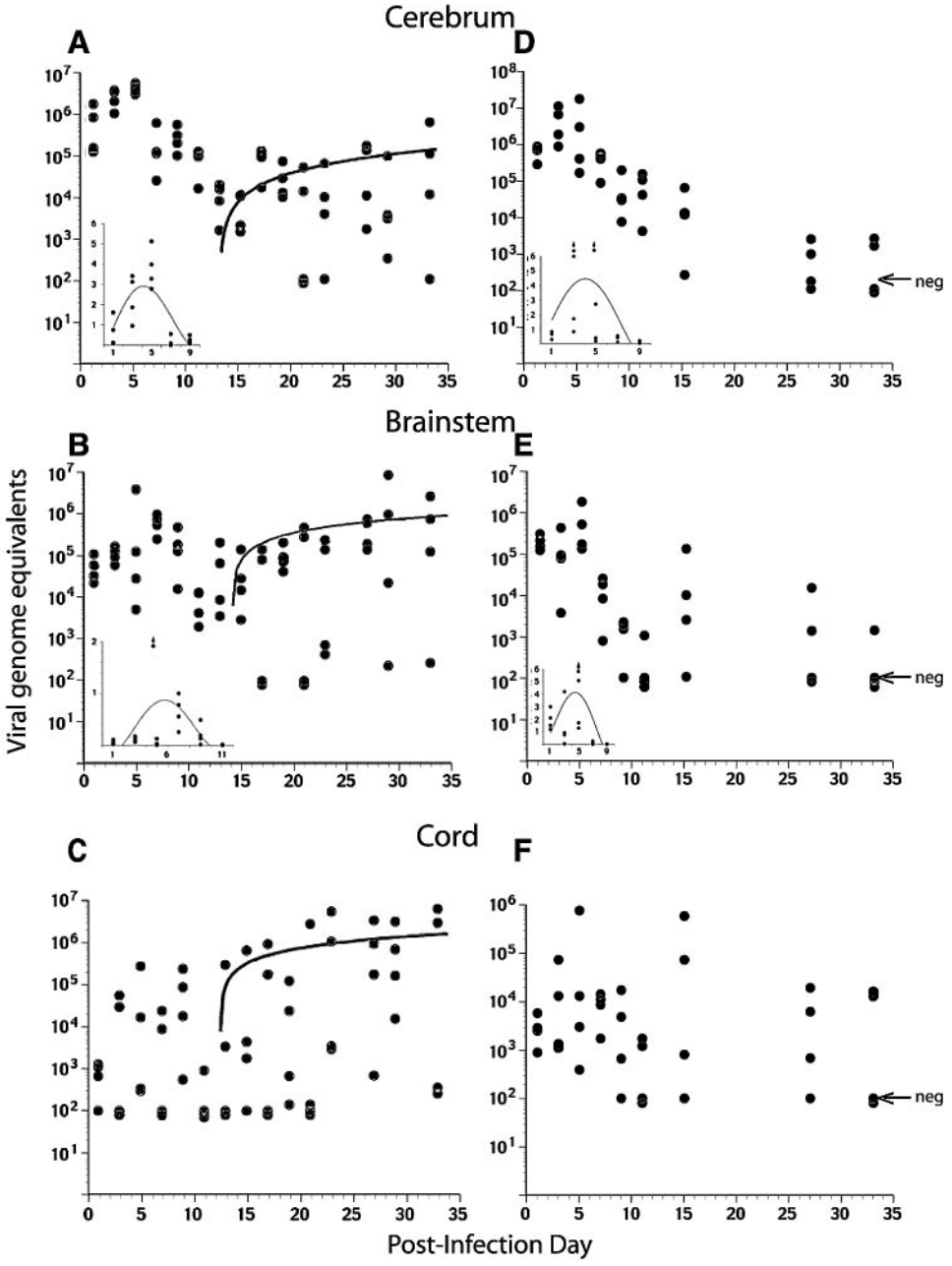


FIG. 1. Kinetics of BeAn viral RNA replication in cerebrums (A and D), brain stems (B and E), and spinal cords (C and F) of susceptible SJL/J (A, B, and C) and resistant B6 (D, E, and F) mice. Data are plotted as numbers of viral RNA copy equivalents per microgram of total RNA, with each open circle representing one mouse. Linear regression of the increase in viral RNA copies between days 11 and 33 p.i. in SJL/J mice is shown with dark lines (note the logarithmic scale of the *y* axis). Insets in the lower left corner of some panels show arithmetic plots of the acute kinetics of viral RNA growth ($10^6$ for A and E; $10^5$ for B and E). The detection limit of the assay was >100 viral RNA copy equivalents.

replication and the levels of RNA produced are similar for SJL/J and B6 mice during acute infection, but that the levels become high only in the spinal cords of susceptible SJL/J mice after 13 days p.i. Moreover, the copy numbers of viral RNA in the spinal cords of mice correlate with the levels of proinflammatory cytokines, suggesting that viral replication levels are a critical determinant for inducing virus-specific T-cell-mediated immune responses and proinflammatory mediators leading to demyelinating disease.

## MATERIALS AND METHODS

**Animals and viral inoculations.** Female SJL and B6 mice were purchased from Jackson Laboratory (Bar Harbor, Maine) or Harlan Laboratories (Indianapolis, Ind.) and were caged and maintained according to the American Association for Accreditation of Laboratory Animal Care standards. Six-week-old mice were anesthetized intraperitoneally with pentobarbital and were inoculated in the right cerebral hemisphere (i.c.) with $2 \times 10^6$ PFU of BeAn virus. Clinical disease scores were assigned as follows: 0, no clinical signs; 1+, mild waddling gait; 2+, severe waddling gait; 3+, severe waddling gait and impaired righting due to extensor spasms; and 4+, complete hindlimb paralysis.

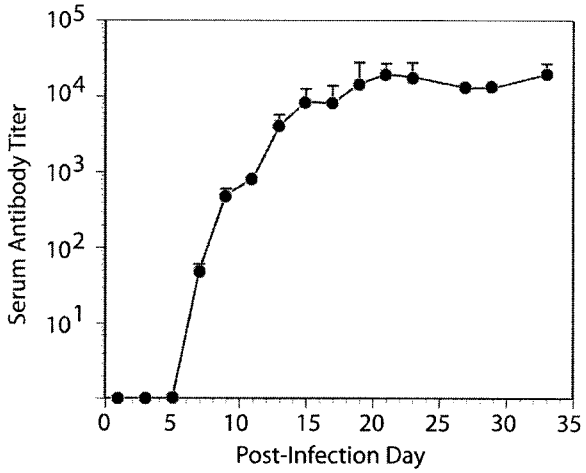


FIG. 2. Virus-specific antibody titers in sera from SJL/J mice. Titers were assayed by ELISAs for the same SJL/J mice that were used to generate the data shown in Fig. 1. Anti-TMEV antibody titers in mouse sera at each time ($n = 4$) are plotted as means ± standard deviations (SD).

**Total RNA isolation.** Spinal cords and brains were removed from mice as described previously (49, 50). Briefly, brain stems were separated from the cerebral hemispheres, and along with the spinal cords, were snap-frozen in liquid nitrogen and stored at −80°C. Tissue pieces were placed in Trizol solution (Gibco) and homogenized (Polytron; Beckman Instruments), and total RNAs were purified according to the manufacturer's recommendations. The quality of the total RNAs was assessed by either RT-PCR for mouse glyceraldehyde-3-phosphate dehydrogenase (GAPDH) mRNA or RNase protection assays for mouse GAPDH and L32 mRNAs. Total RNAs were quantitated by spectrophotometry (absorbance at 260 nm) and verified by denaturing agarose gel electrophoresis.

**Real-time RT-PCR.** Real-time RT-PCRs were performed with mouse total RNAs by use of the Applied Biosystems 5700 sequence detection system as described previously (50). The total RNA from an uninfected mouse brain or spinal cord was used as a control. In vitro-transcribed BeAn virus RNA was used to construct a standard curve for the quantitation of viral RNAs in tissue samples.

**RNase protection assays.** RNase protection assays were used to determine the relative abundance of specific cytokine and chemokine mRNAs in infected and uninfected mouse tissues. $^{32}$P-labeled RNA probes were synthesized by use of a RiboQuant in vitro transcription kit and a RiboQuant multiprobe template set (BD Pharmingen). Probe set 1 allowed the synthesis of radiolabeled probes specific for cytokine mRNAs encoding interleukin-12 (IL-12) p35, IL-12 p40, IL-2, IL-4, IL-6, tumor necrosis factor alpha (TNF-α), and gamma interferon (IFN-γ) as well as mRNAs encoding the mouse housekeeping proteins GAPDH and L32. Probe set 2 enabled the synthesis of probes for RANTES, IL-10, macrophage inflammatory protein 1β (MIP-1β), MIP-1α, IFN-β, IL-18, and MCP-1 (CCL-2) along with mouse GAPDH and L32. The probes were mixed with 40 μg of total RNAs from cerebral hemispheres or mouse spinal cords, heated to 90°C for 1 min, slowly cooled to 56°C over a period of 1 h, and incubated overnight at 56°C. RNA-probe mixtures were treated with RNases according to the RiboQuant RPA kit protocol. RNase-treated samples were electrophoresed in 5% polyacrylamide–8 M urea sequencing gels at 35 W for approximately 1 h, and the gels were dried and analyzed with a Molecular Dynamics Storm phosphorimager.

**Antibody determinations by ELISA.** An enzyme-linked immunosorbent assay (ELISA) was used to determine the antibody titers in sera as described previously (28). Briefly, the wells of microtiter plates (96 wells) were coated with a BeAn virus-infected BHK-21 cell lysate in 0.05 M $NaHCO_3$ buffer, pH 9.6, for 2 h at 24°C, washed with PBS containing 0.02% Tween 20 (PBS-T), incubated with PBS–5% bovine serum albumin overnight at 4°C, and washed again with PBS-T. Duplicate serial twofold serum dilutions were applied to wells, which were then incubated for 1 h at 24°C, washed three times with PBS-T, incubated with goat anti-mouse–horseradish peroxidase (Pierce) at a 1:4,000 dilution in PBS for 1 h at 24°C, washed again, and developed by the use of SigmaFAST OPD reagents according to the manufacturer's recommendations. The plates were read at 490 nm with a Molecular Devices Vmax kinetic microplate reader.

**Statistics.** The numbers of BeAn virus RNA genome equivalents over time (days p.i.) were analyzed by linear regression and plotted on a $\log_{10}$ scale for virus genomes to obtain the best-fit linear regression line. Cytokine and chemokine mRNA expression levels over time for mice with viral genome levels above the threshold were analyzed by the use of Pearson's correlation coefficient. The paired Student's $t$ test was used to compare groups, and differences were considered significant at $P$ values of $<0.05$.

## RESULTS

**Kinetics of active BeAn RNA replication in the CNS of susceptible SJL/J mice leading to viral persistence.** In contrast to the low infectious virus titers of TMEV, viral RNA equivalents are present at extremely high levels in the spinal cords of mice during persistence (49). To analyze in detail the temporal progression of viral RNA replication during the acute phase of infection leading to persistent infection, we inoculated SJL/J mice i.c. with $2 \times 10^6$ PFU of BeAn virus and measured the numbers of virus genomes in their cerebral hemispheres, brain stems, and spinal cords by real-time RT-PCR on alternate days from days 1 to 33 p.i. (Fig. 1A to C). Viral replication was detected in the cerebral hemispheres on day 1 p.i., peaked on day 5 p.i., and declined 1,000-fold by days 11 to 13 p.i. (Fig. 1A). From day 11 p.i. at the end of the acute phase to the persistent phase, there was a trend of increasing RNA viral genome levels, as evidenced by linear regression analysis, that was not significant ($P > 0.05$). However, a substantial variability among individual mice, including four mice with undetectable levels, was observed; the inset in Fig. 1A shows a linear plot of the kinetics of virus growth. On day 33 p.i., viral RNA levels in the cerebral hemispheres of SJL/J mice ranged from undetectable (<100 copies) to $8 \times 10^5$ copies/μg of total RNA (Fig. 1A). Similar but slightly delayed kinetics with fivefold lower viral genome levels were observed for the brain stems; however, much more variability was seen among individual mice (Fig. 1B). The increase in viral RNA levels in the brain stems on days 11 to 33 p.i. was significant ($P < 0.03$).

Compared to the viral RNA levels in the cerebral hemispheres and brain stems, those in the spinal cords were lower and even more variable between days 1 and 11 p.i., with undetectable amounts of viral RNA in one-third of the specimens (Fig. 1C). From days 11 to 33 p.i., the viral RNA copy numbers increased some 50- to 100-fold ($P < 0.005$), and in >80% of the specimens there were detectable levels of viral RNA. These results indicate an active process of viral RNA replication in the spinal cord, and to a lesser extent, in the brain stem; nevertheless, for some mice, the viral RNA levels remained relatively low ($<10^4$ genomes/μg of total RNA), even as late as day 33 p.i. (Fig. 1C).

**Kinetics of BeAn RNA replication in the CNS of resistant B6 mice.** TMEV-induced demyelinating disease has a strong genetic component, with some inbred mouse strains showing marked resistance to the disease (8, 29). Thus, resistant B6 mice were also infected, and the viral RNA copy numbers in their tissues were determined. The acute viral RNA growth kinetics in the cerebral hemispheres of B6 and SJL/J mice were similar (compare Fig. 1A and D). In contrast to the kinetics in SJL/J mice, viral RNAs in B6 mice declined to low levels after day 11 p.i., with 50% of the mice having undetectable levels

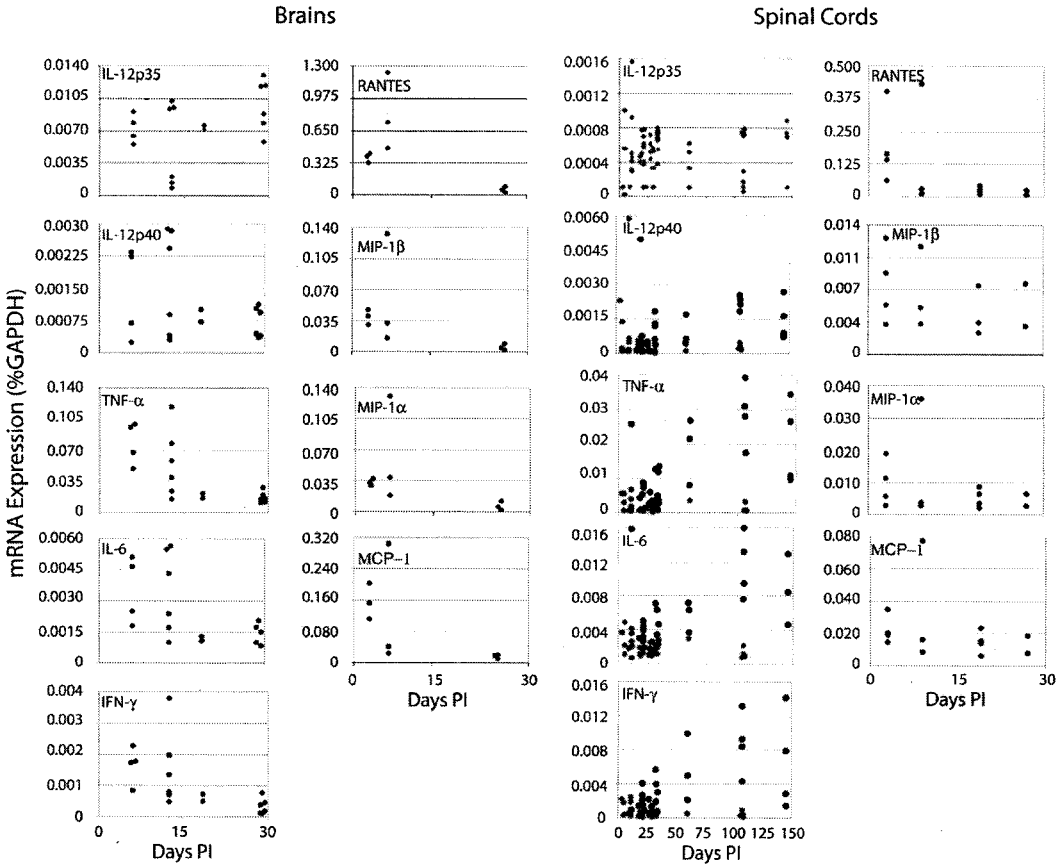


FIG. 3. Proinflammatory cytokine and chemokine mRNA expression levels in brains and spinal cords of BeAn-virus infected SJL/J mice at the indicated times. RNase protection assays revealed an acute increased expression of cytokine and chemokine mRNAs in brains and spinal cords. Both cytokine and chemokine mRNA expression levels decreased in the brain thereafter. While the expression of selective cytokine mRNAs increased, chemokine expression decreased in spinal cords during the transition phase.

between days 27 and 33 p.i. On day 100 p.i., viral RNAs were undetected in the cerebral hemispheres of four B6 mice (not shown). Similar results were observed for the brain stems of B6 mice (Fig. 1E). In the spinal cords, the viral RNA copy numbers were more variable among individual mice, with higher levels of viral RNA at some early times (Fig. 1F). Viral RNA levels seemed to plateau after day 11 p.i., and at day 100 p.i., only two of four mice had detectable viral RNAs in their spinal cords, both of which contained <1,000 viral genomes/μg of total RNA (not shown). Together, these data indicate that there is active viral RNA replication during the transition from the acute to the persistent phase of infection only for susceptible SJL/J mice, not for resistant B6 mice, in which TMEV does not persist.

**Virus-specific serum antibody responses were similar for all mice.** The wide variation in viral genome levels among individual mice after day 11 and the importance of antibody clearance in picornavirus infections suggested that infected mice with high viral genome levels may have mounted less brisk virus-specific antibody responses. Thus, the production of TMEV-specific antibodies was determined for sera from TMEV-infected SJL/J mice by the use of ELISAs (Fig. 2). TMEV-specific antibody titers were first detected on day 7 p.i. (mean titer, ~1:100) and increased steadily until reaching a plateau by day 19 p.i. (mean titer, ~1:10,000) (Fig. 2). The rise in antibody titers corresponded to the fall in viral RNA levels observed for the cerebral hemispheres and brain stems of infected mice (Fig. 1A and B). Virus-specific antibody titers were similar for all mice tested at each time point p.i. and did not correlate with the viral genome load. Antibody responses to TMEV infection were robust in all mice, suggesting that antibody responses play a lesser role in suppressing viral replication in the spinal cord.

**Proinflammatory cytokine mRNA expression levels increase in SJL/J spinal cords during the transition to CNS viral persistence.** Since acute viral replication was similar in both resistant and susceptible mice, the transition from the acute to the chronic phase of TMEV infection appears to be critical for the development of demyelinating disease. To provide insight into this process, we assessed the expression of several proinflammatory cytokine mRNAs (5, 46) by performing RNase protection assays with the SJL/J brains and spinal cords used to generate the data shown in Fig. 1 and with additional SJL/J spinal cords collected on days 60, 107, and 145 p.i. In the brain, both SJL/J and B6 mice displayed similar patterns of cytokine mRNA expression (Fig. 3; also see Fig. S1 in the supplemental material). On day 107 p.i., cytokine expression was low in resistant B6 brains but remained high in some susceptible SJL/J brains (not shown). TNF-α and IFN-γ were the most

highly expressed cytokines in the spinal cords of SJL/J mice, with even higher levels observed at later times p.i. (Fig. 3). These are the cytokines that are expected to be elevated for a $CD4^+$ Th1 T-cell-mediated immunopathology, as previously reported (5, 46). In addition, the levels of IL-6 mRNA produced by macrophages were also high (20). For semisusceptible SJL/J mice, variability in cytokine mRNA expression in the spinal cord was observed (Fig. 3). B6 spinal cord cytokine mRNA expression levels were studied previously (12), revealing similar acute profiles for both SJL and B6 mice. For that study, cytokine levels were only assayed on day 107 p.i. and were low (not shown). The major difference between resistant and susceptible mice was not the individual cytokines expressed (the same cytokine mRNAs were up-regulated), but rather the levels of expression.

**Cytokine mRNA expression is correlated with a threshold viral genome load.** Variability in proinflammatory cytokine mRNA expression was observed for SJL/J mice, even at late times p.i. (Fig. 3). We therefore compared the cytokine expression levels to the viral genome loads in the spinal cord samples of the individual SJL/J mice used to generate the data shown in Fig. 3. For mice with viral genome loads of $>2.6 \times 10^5$ RNA copies per μg of total RNA, there were significant increases in IFN-γ and TNF-α ($r = 0.62$, $P < 0.001$) as well as IL-6 ($r = 0.48$, $P < 0.01$) expression levels over time (Fig. 4). The viral genome threshold was determined by finding mice with the lowest viral RNA copy numbers but with high cytokine expression levels, e.g., one mouse with high cytokine mRNA expression had a viral genome load of $9.6 \times 10^5$, while another with low cytokine mRNA expression had a viral genome load of $2.6 \times 10^5$. It turned out that all mice with viral genome loads of $>9.6 \times 10^5$ had high cytokine mRNA expression levels while all mice with viral genome loads of $<2.6 \times 10^5$ had low mRNA expression levels. However, there was no discernible correlation between cytokine mRNA levels and genome loads, i.e., cytokine expression levels were always high when viral genome loads exceeded the threshold but were not directly proportionate to the actual viral load. Those mice with genome loads of $<2.6 \times 10^5$ copies had low cytokine expression levels regardless of the time p.i. This finding suggested that increasing IFN-γ, TNF-α, and IL-6 mRNA levels were driven by persistent infections.

**Chemokine mRNA expression only parallels proinflammatory cytokine mRNA expression acutely.** Chemokines are soluble, activation-inducible, proinflammatory molecules that are chemotactic for different cell types and are up-regulated during TMEV infection (21, 34, 42). RNase protection assays were performed to determine the expression levels of chemokine mRNAs during BeAn infections of SJL/J and B6 mice. The chemokine RANTES, which is chemotactic for monocytes and memory T cells, showed the largest increase in mRNA expression levels in the brains of both SJL/J and B6 mice, with its expression being elevated early but decreasing to very low levels after days 7 to 9 p.i. (Fig. 3; also see the supplemental material). A similar temporal trend in expression was observed for MIP-1β, MIP-1α, and MCP-1, although their mRNA levels were lower than those for RANTES. In SJL/J spinal cords, the expression of these chemokines was highest during the acute phase of infection, with lower expression levels after day 9 p.i. (Fig. 3). Previously, chemokine expression was reported to be low in resistant C57BL/10 and B6 cords after the acute phase of infection (34, 42), and the B6 spinal cords were therefore not assayed for this study. Thus, an increase in chemokine expression was not observed in SJL/J cords during the transition to persistent infection, as was seen with cytokine expression.

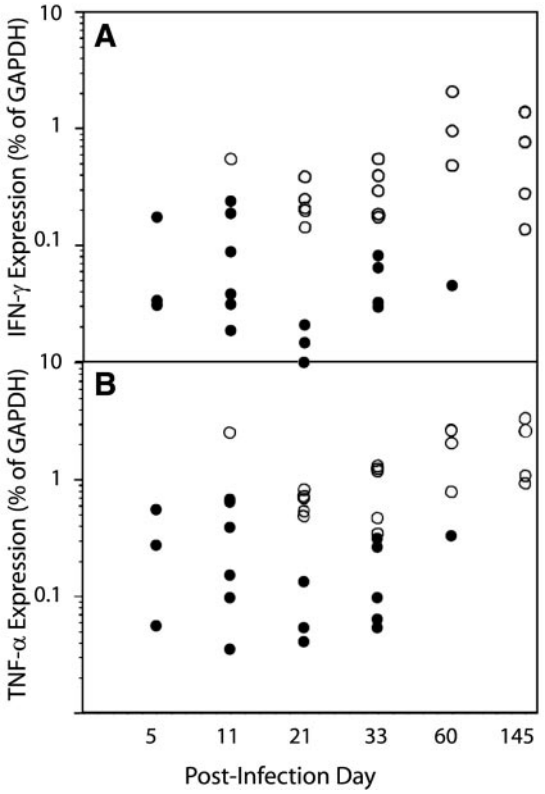


FIG. 4. IFN-γ and TNF-α mRNA expression in spinal cords of BeAn virus-infected SJL/J mice with high and low viral genome levels. A threshold of $2.6 \times 10^5$ viral RNA copy equivalents per μg of total RNA was determined by visual inspection of RNase protection results compared to viral genome copy levels for each sample (see the text). Percentages of IFN-γ (A) and TNF-α (B) expression relative to that of GAPDH on the indicated days p.i. are shown. Mouse spinal cords contained viral genome loads that were higher (○) or lower (●) than a threshold value of $2.6 \times 10^5$ genome copy equivalents per μg of total RNA. Each circle represents one mouse.

**Demyelinating disease is correlated with large genome loads and high cytokine mRNA expression levels.** Although the percentage of BeAn virus-infected SJL/J mice ($n = 27$) that developed demyelinating disease increased with time, approximately 50% of the animals remained clinically normal even at late times p.i. (see Fig. 6). We therefore compared viral genome loads, proinflammatory cytokine expression levels, and clinical disease for nine healthy and five diseased mice (clinical scores, 1+ to 3+) on day 107 p.i. Each of the five diseased mice had a viral genome load in excess of $2 \times 10^7$ per μg of cord total RNA, whereas all but one of the nine healthy infected mice had genome loads that were under the threshold of $2.6 \times 10^5$ per μg of total RNA (Fig. 5). The proinflammatory cytokine level in each mouse was correlated with disease, with an elevated expression of IL-12 p40, TNF-α, IL-6, and IFN-γ mRNAs observed for diseased animals and low levels of these

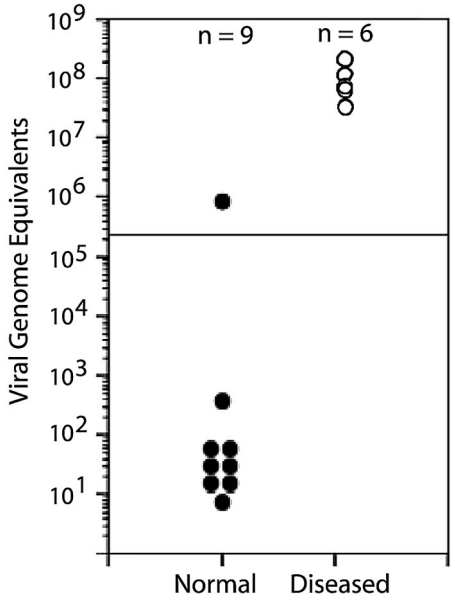


FIG. 5. Viral genome equivalents (copy numbers) in spinal cords of BeAn virus-infected SJL/J mice that were healthy ($n = 9$) or had developed clinical demyelinating disease ($n = 5$) when sacrificed on day 107 p.i. All diseased mice had viral RNA copy numbers of $>2.6 \times 10^5$ (threshold level; horizontal line), and with one exception, all healthy mice had copy numbers of $<2.6 \times 10^5$. The detection limit for this assay was 100 genome copy numbers per μg of total spinal cord RNA.

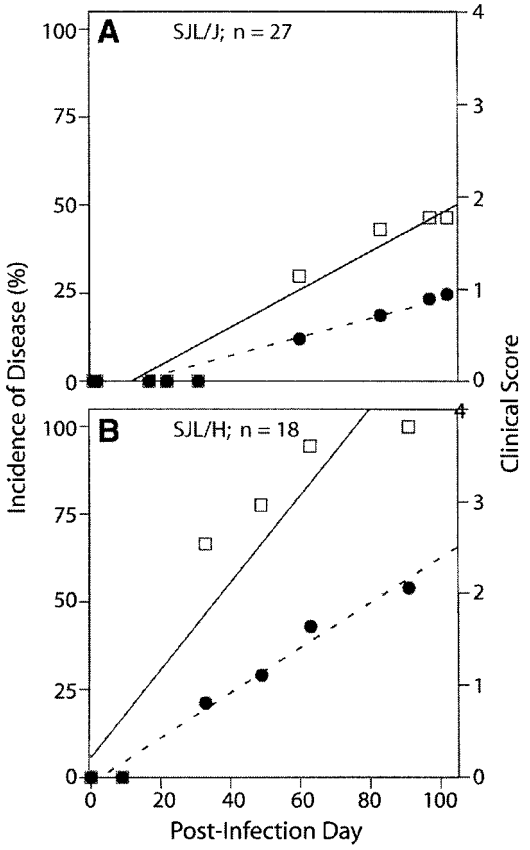


FIG. 6. Comparison of SJL/J and SJL/H mice for susceptibility to TMEV-induced demyelinating disease. Mice from Jackson Laboratory (SJL/J; $n = 27$) (A) and from Harlan Laboratories (SJL/H; $n = 18$) (B) were inoculated i.c. with $2 \times 10^6$ PFU of BeAn virus, and clinical disease was assessed weekly until day 100 p.i. The incidence of clinical disease (left axis [□]) was plotted as the percentages of mice with signs of clinical demyelinating disease. The incidence of disease severity (right axis [●]) was plotted as mean clinical scores for all animals on each day p.i.

cytokines observed for healthy animals (Table 1). These results indicate that high levels of viral RNA replication in the spinal cords of mice are associated with the expression of high levels of IL-12 p40, TNF-α, IL-6, and IFN-γ mRNAs and, in turn, disease progression.

**SJL substrains show differential susceptibilities to TMEV-induced demyelinating disease.** SJL/J mice are usually highly susceptible to TMEV-induced demyelinating disease (10). When SJL/J mice are inoculated i.c. with $>10^6$ PFU of BeAn virus, the progression of demyelinating disease in individual mice is variable, but most animals develop clinical disease by 90 days p.i. (13, 29). During the course of the present study, we found that SJL/J mice were less susceptible to TMEV-induced demyelinating disease than was previously observed. To compare the susceptibility of the SJL/J substrain (from The Jackson Laboratory) with that of the SJL/H substrain (from Harlan Laboratories), we infected mice from both vendors and monitored the disease onset and severity. Figure 6 shows the percentages of mice who were affected and clinical disease scores for mice from both vendors over time. SJL/J mice were clearly less susceptible than SJL/H mice to demyelinating disease, displaying a lower incidence, delayed onset, and less severe clinical scores when monitored until day 100 p.i. Figure 7 shows the viral RNA copy numbers in the brains and spinal cords of the two SJL substrains on days 11 and 33 p.i. Although the mean viral RNA copy numbers in the spinal cords of SJL/H mice were approximately threefold larger than those in SJL/J mice on day 33 p.i., the difference was not significant ($P < 0.05$) due to the variability in viral genome loads among individual animals. In any case, the 30- to 40-fold increase in viral copy numbers in the spinal cords from both substrains between days 11 and 33 p.i. supports the observation of active viral RNA replication during the transition to TMEV persistence (Fig. 1C). Although the reason for the difference in susceptibility of the SJL substrains is unknown, the larger variability among

TABLE 1. Correlation of demyelinating disease with cytokine expression level in BeAn virus-infected SJL/J mice on day 107 p.i.

| Cytokine | % Cytokine expression (mean ± SD)[a] | | Fold increase in diseased mice | $P$ value[b] |
|---|---|---|---|---|
| | Unaffected mice[a] | Diseased mice[a] | | |
| IL-12 p35 | 0.075 ± .001 | 0.013 ± .012 | 0.2 | NS |
| IL-12 p40 | 0.025 ± .012 | 0.221 ± .030 | 8.8 | <0.0001 |
| TNF-α | 0.119 ± .102 | 2.882 ± .892 | 24.2 | <0.0002 |
| IL-6 | 0.112 ± .056 | 1.154 ± .379 | 10.3 | <0.005 |
| IFN-γ | 0.037 ± .029 | 0.876 ± .361 | 23.8 | <0.001 |
| IL-2 | 0.102 ± .007 | 0.145 ± .047 | 1.4 | NS |

[a] Cytokine expression levels were calculated as percentages of GAPDH mRNA expression.
[b] NS, not significant.

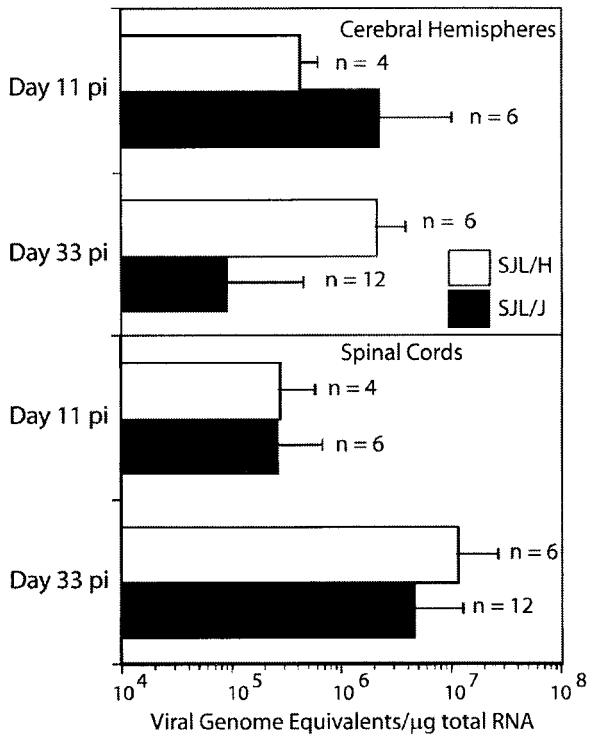


FIG. 7. Comparison of viral genome copy equivalents per microgram of total RNA in the brains and spinal cords of SJL/J and SJL/H mice, as determined by quantitative real-time RT-PCR. The time points shown represent the approximate end of the acute phase of virus infection (day 11 p.i.) and the early persistent phase (day 33 p.i.), when viral genome loads are elevated in spinal cords. Data shown are means ± SD.

individual SJL/J mice allowed an analysis of the association of the viral genome load with the expression of proinflammatory mediators as well as clinical demyelinating disease.

## DISCUSSION

We used real-time RT-PCR and RNase protection assays to quantify the numbers of viral genome copy equivalents and the levels of cytokine and chemokine mRNA expression in the cerebral hemispheres, brain stems, and spinal cords of susceptible SJL/J and resistant B6 mice inoculated i.c. with the BeAn virus strain. Our aim was to characterize in greater detail the acute (days 1 to 11 p.i.) and transitional (days 13 to 33 p.i.) phases of TMEV infection of the CNS leading to viral persistence (>day 30 p.i.). SJL/J mice, which turned out to be less susceptible to TMEV-induced demyelinating disease than was previously reported, were also examined at later times for comparisons of viral genome loads and cytokine mRNA expression levels with the presence of clinical disease. The principal findings of this study were as follows: (i) there is an association between TMEV CNS infection and increasing viral RNA copy numbers during the transition to persistent infection, suggesting that viral persistence is not merely due to incomplete viral clearance; and (ii) there is an association between high cytokine mRNA expression levels and clinical demyelinating disease.

For acute infections, the kinetics and levels of viral RNA replication in the cerebral hemispheres of susceptible SJL/J and resistant B6 mice were similar (Fig. 1A and D), as were the types and levels of proinflammatory cytokine and chemokine mRNAs (Fig. 3) (12, 34, 42, 46), although after day 11 mRNA expression in brains for both virus strains decreased to low levels (Fig. 7). The similarities in viral RNA replication and in cytokine and chemokine expression profiles in the brains of both susceptible SJL/J and resistant B6 mice suggests that TMEV RNA replication in the brain, while necessary for initial amplification and spread of the virus from the site of inoculation to the spinal cord, is not sufficient for the development of TMEV persistence and demyelinating disease.

It was previously found that TMEV RNA copy numbers rise to extremely high levels ($10^8$ per μg of total RNA) during persistent infections (>day 30 p.i.), while infectious virus titers fall to very low levels in the spinal cords of SJL mice (49). Most animals in that study were sacrificed after day 30 p.i. and had clinical signs of demyelinating disease, but relatively few mice were examined during the acute phase of infection (49). With this study, we have shown that the numbers of viral genomes in the spinal cords of some SJL/J mice increased to levels comparable to those observed in the earlier study, while viral RNA levels in some mice remained low, even as late as day 33 p.i. (Fig. 1). Since BeAn virus-infected SJL/J mice were not clinically diseased by day 33 p.i., no correlation between the viral genome load and disease could be discerned. Instead, we analyzed the expression levels of proinflammatory cytokine and chemokine mRNAs to gain insights into the relationship between viral replication and virus-specific cellular immune responses. For all mice tested, whether they were resistant or susceptible, similar cytokine and chemokine mRNAs were upregulated. The major difference between individual animals was the respective level of mRNA expression. Mice with high viral genome loads expressed the highest cytokine mRNA levels. Quantitation by real-time RT-PCR identified a threshold level of $2.6 \times 10^5$ viral genome copies per μg of total RNA from the spinal cord; mice with viral genome levels in the spinal cord that were higher than the threshold had high proinflammatory cytokine expression levels, while mice with genome levels at or below the threshold had low chemokine expression levels. These results support a direct link between the level of CNS viral persistence, the virus-specific T-cell response, and the synthesis of proinflammatory mediators.

Recently, Ransohoff et al. (42) reported that TMEV persistence (measured in infectious virus titers) is the major determinant for chronic chemokine expression in wild-type as well as $CD4^{-/-}$ and $CD8^{-/-}$ resistant B6 and susceptible PLJ mice. RANTES, IP-10, and MCP-1 levels were elevated, according to real-time RT-PCR, in mice with virus persistence in the spinal cord. Previously, Karpus et al. (21) had found that MIP-1α and MCP-1 levels were increased, according to ELISAs, in persistently infected SJL mice. In the present study, mice with low chemokine mRNA expression levels often showed detectable viral RNA copy numbers in the spinal cord, indicating that viral persistence alone was not sufficient to induce high levels of chemokine expression. However, the level of viral genomes in the cord appeared to be critical for maximum cytokine mRNA expression.

TMEV persistence occurs as a result of active viral RNA

replication and a concomitant incomplete clearance of the virus from the CNS (Fig. 1). TMEV persists even in the presence of a strong virus-specific immunoglobulin G2a (IgG2a) antibody response (40) and in the absence of RNA mutations that would allow the virus to escape neutralization (45). For the transition from an acute to a persistent infection in SJL/J mice, we found no correlation between virus-specific ELISA titers and viral genome loads (Fig. 1 and 2). Although virus-specific T-cell responses were not examined in this study, previous analyses demonstrated that virus-specific $CD8^+$ cytotoxic T lymphocytes (CTLs), especially those specific for an immunodominant $VP2_{121-130}$ epitope, account for acute TMEV clearance in resistant B6 mice (7, 18, 32). In contrast to the early appearance and rapid increase in CTL activity in resistant B6 mice, such activity appears late in susceptible SJL mice and remains at low levels (17), suggesting that viral persistence in SJL mice is due to insufficient virus-specific CTL activity. Genetic studies have also shown that resistance to TMEV-induced demyelinating disease is linked to the H-2D major histocompatibility complex class I locus (14, 29, 43), further suggesting that altered CTL responsiveness is a contributor to susceptibility. However, Kang et al. (24, 25) more recently demonstrated not only that SJL mice generate virus-specific $CD8^+$-T-cell responses equivalent to those of B6 mice, but also that CNS-infiltrating $CD8^+$ T cells in SJL mice are fully functional virus-specific effector cells. Thus, TMEV CNS persistence may not be due to a lack of virus-specific CTL activity. Alternatively, major histocompatibility complex class I-restricted T cells may influence susceptibility through a $CD8^+$-T-cell regulatory activity (36, 37). In that case, susceptible SJL mice should generate less efficient $CD8^+$ regulation of virus-specific $CD4^+$ T cells than that generated by resistant B6 mice, which in fact has been shown for susceptible versus resistant BALB/c substrains (26). Thus, reduced $CD8^+$-T-cell regulation may lead to increased virus-specific $CD4^+$-T-cell delayed-type hypersensitivity and the recruitment of monocytes into the CNS, continuously providing macrophages that are susceptible to infection (leading to higher viral RNA genomes in the present study) and effector macrophages that damage myelin. Consistent with this hypothesis, Aubagnac et al. (1) found by Northern hybridization that DA virus-infected SJL/J mice with an inactivated β2*m* gene (SJL/J $\beta2m^{-/-}$) had significantly increased amounts of spinal cord viral RNA on day 45 p.i. compared to wild-type mice (SJL/J $\beta2m^{+/+}$). Increased persistence in the CNS would also explain the enhanced susceptibility and more severe demyelinating pathology seen for CD8-deficient mice than for wild-type SJL mice (4).

TMEV provides a highly relevant experimental animal model of the human demyelinating disease MS. A viral infection in individuals who are genetically predisposed to MS is believed to trigger autoimmune myelin damage (31, 48). It is not known whether an acute infection suffices or whether the infection must be chronic. Miller et al. (33) detected epitope spreading in the Theiler's virus model system, in which virus damage led to the activation of autoreactive T cells that were specific for myelin protein epitopes. For this infection, virus-specific $CD4^+$-T-cell responses are observed within 7 days p.i., increasing to high levels by day 30 p.i. and persisting for >300 days p.i. (13), while myelin-specific $CD4^+$ Th1 T-cell responses are not detected until 50 to 60 days p.i. (27, 33), or about 40 days after demyelination is first observed (15). Thus, myelin breakdown in TMEV-induced demyelinating disease in mice is initiated by bystander damage from virus-specific, $CD4^+$ Th1 T-cell-mediated delayed-type hypersensitivity (13), and autoimmunity arises after myelin damage has already occurred (27, 33). The role of TMEV persistence after the onset of autoimmunity has not been addressed. Although autoimmunity may be an epiphenomenon, i.e., not responsible for tissue damage, Neville et al. (35) found that tolerance induced between days 23 and 70 p.i. by peripheral administration of a fusion peptide of myelin basic protein and proteolipid protein immunodominant epitopes significantly reduced TMEV-induced clinical and demyelinating disease during that period. Thus, autoimmunity may account for at least a portion of spinal cord damage (25% reduction in clinical disease scores compared to those for control mice who were made tolerant by the use of bovine serum albumin) (35).

In a recent study, a transient inhibition of CD154 in BeAn virus-infected SJL mice beginning on day 21 p.i. that reduced demyelinating disease was associated with increased virus titers in the brain and spinal cord (40- and 12-fold compared to titers for control antibody-treated mice) at one time point (day 70 p.i.) (22). Higher infectious virus titers in the brain than in the spinal cord would be expected when immunosuppression of the host affects TMEV clearance (38, 49), suggesting that the CD154 blockade may have affected viral clearance. The results of the present study suggest that high viral genome loads during TMEV persistence, together with high levels of proinflammatory cytokines, are required to "drive" demyelinating disease. Evidence that autoimmunity can be self-perpetuating over many months in this model is still lacking. It will be important to determine whether antiviral agents are more effective than immunomodulatory ones, i.e., those inducing tolerance to myelin protein epitopes, for treating TMEV-induced demyelinating disease in mice. However, such studies await the availability of efficient inhibitors of cardioviruses.

## ACKNOWLEDGMENTS

We thank Patricia Kallio for technical assistance and Mary Lou Jelachich for helpful discussions.

This work was supported by NIH grant NS21913.

## REFERENCES

1. **Aubagnac, S., M. Brahic, and J.-F. Bureau.** 2001. Viral load increases in SJL/J mice persistently infected by Theiler's virus after inactivation of the β2m gene. J. Virol. **75:**7723–7726.
2. **Aubert, C., and M. Brahic.** 1995. Early infection of the central nervous system by the GDVII and DA strains of Theiler's virus. J. Virol. **69:**3197–3200.
3. **Aubert, C., M. Chamorro, and M. Brahic.** 1987. Identification of Theiler's virus infected cells in the central nervous system of the mouse during demyelinating disease. Microb. Pathog. **3:**319–326.
4. **Begolka, W. S., L. M. Haynes, J. K. Olson, J. Padilla, K. L. Neville, M. C. Dal Canto, J. P. Palma, B. S. Kim, and S. D. Miller.** 2001. CD8-deficient SJL mice display enhanced susceptibility to Theiler's virus infection and increased demyelinating pathology. J. Neurovirol. **7:**409–420.
5. **Begolka, W. S., C. L. Vanderlugt, S. M. Rahbe, and S. D. Miller.** 1999. Differential expression of inflammatory cytokines parallels progression of central nervous system pathology in two clinically distinct models of multiple sclerosis. J. Immunol. **161:**4437–4446.
6. **Blakemore, W. F., C. J. Welsh, P. Tonks, and A. A. Nash.** 1988. Observations on demyelinating lesions induced by Theiler's virus in CBA mice. Acta Neuropathol. **76:**581–589.
7. **Borson, N. D., C. Paul, X. Lin, W. K. Nevala, M. A. Strausbauch, M. Rodriguez, and P. J. Wettstein.** 1997. Brain-infiltrating cytolytic T lymphocytes specific for Theiler's virus recognize $H2D^b$ molecules complexed with

a viral VP2 peptide lacking a consensus anchor residue. J. Virol. **71:**5244–5250.
8. **Brahic, M., and J.-F. Bureau.** 1998. Genetics of susceptibility to Theiler's virus infection. BioEssays **20:**627–633.
9. **Brahic, M., W. G. Stroop, and J. R. Baringer.** 1981. Theiler's virus persists in glial cells during demyelinating disease. Cell **126:**123–128.
10. **Bureau, J.-F., X. Montagutelli, S. Lefebvre, J. L. Guenet, M. Pla, and M. Brahic.** 1992. The interaction of two groups of murine genes determines the persistence of Theiler's virus in the central nervous system. J. Virol. **66:**4698–4704.
11. **Chamorro, M., C. Aubert, and M. Brahic.** 1986. Demyelinating lesions due to Theiler's virus are associated with ongoing central nervous system infection. J. Virol. **57:**992–997.
12. **Chang, J. R., E. Zaczynska, C. D. Katsetos, C. D. Platsoucas, and E. L. Oleszak.** 2000. Differential expression of transforming growth factor beta, interleukin-2, and other cytokines in the central nervous system of Theiler's murine encephalitis virus-infected susceptible and resistant strains of mice. J. Virol. **278:**346–360.
13. **Clatch, R. J., H. L. Lipton, and S. D. Miller.** 1986. Characterization of Theiler's murine encephalomyelitis virus (TMEV)-specific delayed-type hypersensitivity responses in TMEV-induced demyelinating disease: correlation with clinical signs. J. Immunol. **136:**920–926.
14. **Clatch, R. J., R. W. Melvold, S. D. Miller, and H. L. Lipton.** 1985. Theiler's murine encephalomyelitis virus (TMEV)-induced demyelinating disease in mice is influenced by the H-2D region: correlation with TMEV-specific delayed-type hypersensitivity. J. Immunol. **135:**1408–1414.
15. **Dal Canto, M. C., and H. L. Lipton.** 1976. Primary demyelination in Theiler's virus infection. An ultrastructural study. Lab. Investig. **33:**626–637.
16. **Dal Canto, M. C., and H. L. Lipton.** 1982. Ultrastructural immunohistochemical localization of virus in acute and chronic demyelinating Theiler's virus infection. Am. J. Pathol. **106:**20–29.
17. **Dethlefs, S., M. Brahic, and E.-L. Larsson-Sciard.** 1997. An early, abundant cytotoxic T-lymphocyte response against Theiler's virus is critical for preventing viral persistence. J. Virol. **71:**8875–8878.
18. **Dethlefs, S., N. Escriou, M. Brahic, S. van der Werf, and E.-L. Larsson-Sciard.** 1997. Theiler's virus and Mengo virus induce cross-reactive cytotoxic T lymphocytes restricted to the same immunodominant VP2 epitope in C57BL/6 mice. J. Virol. **71:**5361–5365.
19. **Gerety, S. J., K. M. Rundell, M. C. Dal Canto, and S. D. Miller.** 1994. Class II-restricted T cell responses in Theiler's murine encephalomyelitis virus-induced demyelinating disease. VI. Potentiation of demyelination with and characterization of an immunopathologic $CD4^+$ T cell line specific for an immunodominant VP2 epitope. J. Immunol. **152:**919–929.
20. **Hirano, T.** 1998. Interleukin-6 and its receptor: 10 years later. Int. Rev. Immunol. **16:**249–284.
21. **Hoffman, L. M., B. T. Fife, W. S. Begolka, S. D. Miller, and W. J. Karpus.** 1999. Central nervous system chemokine expression during Theiler's virus-induced demyelinating disease. J. Neurovirol. **5:**635–642.
22. **Howard, L. M., K. L. Neville, L. M. Haynes, M. C. Dal Canto, and S. D. Miller.** 2003. CD154 blockade results in transient reduction in Theiler's murine encephalomyelitis virus-induced demyelinating disease. J. Virol. **77:**2247–2250.
23. **Jelachich, M. L., and H. L. Lipton.** 1999. Restricted Theiler's murine encephalomyelitis virus infection in murine macrophages induces apoptosis. J. Gen. Virol. **80:**1701–1705.
24. **Kang, B.-S., M. A. Lyman, and B. S. Kim.** 2002. Differences in avidity and epitope recognition of $CD8^+$ T cells infiltrating the central nervous system of SJL/J mice infected with BeAn and DA strains of Theiler's murine encephalomyelitis virus. J. Virol. **76:**11780–11784.
25. **Kang, B.-S., M. A. Lyman, and B. S. Kim.** 2002. The majority of infiltrating $CD8^+$ T cells in the central nervous system of susceptible SJL/J mice infected with Theiler's virus are virus specific and fully functional. J. Virol. **76:**6577–6585.
26. **Karls, K. A., F. W. Denton, and R. W. Melvold.** 2002. Susceptibility to Theiler's murine encephalomyelitis virus-induced demyelinating disease in BALB/cANCr mice is related to absence of a $CD4^+$ subset. Multiple Sclerosis **8:**469–474.
27. **Katz-Levy, Y., K. L. Neville, J. Padilla, S. Rahbe, W. S. Begolka, A. M. Girvin, J. K. Olson, C. L. Vanderlugt, and S. D. Miller.** 2000. Temporal development of autoreactive Th1 responses and endogenous presentation of self myelin epitopes by central nervous system-resident APCs in Theiler's virus-infected mice. J. Immunol. **165:**5304–5314.
28. **Lipton, H. L., A. Friedmann, P. Sethi, and J. R. Crowther.** 1998. Characterization of Vilyuisk virus, a cause of human encephalitis in Russia. J. Med. Virol. **12:**195–204.
29. **Lipton, H. L., and R. Melvold.** 1984. Genetic analysis of susceptibility to Theiler's virus-induced demyelinating disease in mice. J. Immunol. **132:**1821–1825.
30. **Lipton, H. L., G. Twaddle, and M. L. Jelachich.** 1995. The predominant virus antigen burden is present in macrophages in Theiler's murine encephalomyelitis virus (TMEV)-induced demyelinating disease. J. Virol. **69:**2525–2533.
31. **Markovic-Plese, S., and H. F. McFarland.** 2001. Immunopathogenesis of the multiple sclerosis lesion. Curr. Neurol. Neurosci. Rep. **1:**257–262.
32. **Mendez-Fernandez, Y. V., A. J. Johnson, M. Rodriguez, and L. R. Pease.** 2003. Clearance of Theiler's virus infection depends on the ability to generate a $CD8^+$ T cell response against a single immunodominant viral peptide. Eur. J. Immunol. **33:**2501–2510.
33. **Miller, S. D., C. VanderLugt, W. S. Begolka, W. Pao, R. L. Yauch, K. L. Neville, Y. Katz-Levy, A. Carrizosa, and B. S. Kim.** 1997. Persistent infection with Theiler's virus leads to CNS autoimmunity via epitope spreading. Nat. Med. **3:**1113–1136.
34. **Murray, P. D., K. Krivacic, A. Chernosky, T. Wei, R. M. Ransohoff, and M. Rodriguez.** 2000. Biphasic and regionally-restricted chemokine expression in the central nervous system in the Theiler's virus model of multiple sclerosis. J. Neurovirol. **6:**S44–S52.
35. **Neville, K. L., J. Padilla, and S. D. Miller.** 2002. Myelin-specific tolerance attenuates the progression of a virus-induced demyelinating disease: implications for the treatment of MS. J. Neuroimmunol. **123:**18–29.
36. **Nicholson, S. M., M. C. Dal Canto, S. D. Miller, and R. W. Melvold.** 1996. Adoptively transferred $CD8^+$ T lymphocytes provide protection against TMEV-induced demyelinating disease in BALB/c mice. J. Immunol. **156:**1276–1283.
37. **Nicholson, S. M., J. D. Peterson, S. D. Miller, K. Wang, M. C. Dal Canto, and R. W. Melvold.** 1994. BALB/c substrain differences in susceptibility to Theiler's murine encephalomyelitis virus-induced demyelinating disease. J. Neuroimmunol. **52:**19–24.
38. **Njenga, M. K., K. Asakura, S. F. Hunter, P. Wettstein, L. R. Pease, and M. Rodriguez.** 1997. The immune system preferentially clears Theiler's virus from the gray matter of the central nervous system. J. Virol. **71:**8592–8601.
39. **Ohara, Y., S. Stein, J. Fu, L. Stillman, L. Klaman, and R. P. Roos.** 1988. Molecular cloning and sequence determination of DA strain of Theiler's murine encephalomyelitis virus. Virology **164:**245–255.
40. **Peterson, J. D., C. Waltenbaugh, and S. D. Miller.** 1992. IgG subclass responses to Theiler's murine encephalomyelitis virus infection and immunization suggest a dominant role for Th1 cells in susceptible mouse strains. Immunology **75:**652–658.
41. **Pevear, D. C., M. Calenoff, E. Rozhon, and H. L. Lipton.** 1987. Analysis of the complete nucleotide sequence of the picornavirus Theiler's murine encephalomyelitis virus indicates that it is closely related to cardioviruses. J. Virol. **61:**1507–1516.
42. **Ransohoff, R. M., T. Wei, K. D. Pavelko, P. D. Lee, P. D. Murray, and M. Rodriguez.** 2002. Chemokine expression in the central nervous system of mice with viral disease resembling multiple sclerosis: Roles of $CD4^+$ and $CD8^+$ T cells and viral persistence. J. Virol. **76:**2217–2224.
43. **Rodriguez, M., J. Leibowitz, and C. S. David.** 1986. Susceptibility to Theiler's virus-induced demyelination. Mapping of the gene within the H-2D region. J. Exp. Med. **163:**620–631.
44. **Rodriguez, M., J. L. Leibowitz, and P. W. Lampert.** 1983. Persistent infection of oligodendrocytes in Theiler's virus-induced encephalomyelitis. Ann. Neurol. **13:**426–433.
45. **Rozhon, E. J., J. D. Kratochvil, and H. L. Lipton.** 1983. Analysis of genetic variation in Theiler's virus during persistent infection in the mouse central nervous system. Virology **128:**16–32.
46. **Sato, S., S. L. Reiner, M. A. Jensen, and R. P. Roos.** 1997. Central nervous system cytokine mRNA expression following Theiler's murine encephalomyelitis virus infection. J. Neuroimmunol. **76:**213–223.
47. **Simas, J. P., and J. K. Fazakerley.** 1996. The course of disease and persistence of virus in the central nervous system varies between individual CBA mice infected with the BeAn strain of Theiler's murine encephalomyelitis virus. J. Gen. Virol. **77:**2701–2711.
48. **Steinman, L., R. Martin, C. Bernard, P. Conlon, and J. R. Oksenberg.** 2002. Multiple sclerosis: deeper understanding of its pathogenesis reveals new targets for therapy. Annu. Rev. Neurosci. **25:**491–505.
49. **Trottier, M., P. Kallio, W. Wang, and H. L. Lipton.** 2001. High numbers of viral RNA copies in the central nervous system of mice during persistent infection with Theiler's virus. J. Virol. **75:**7428.
50. **Trottier, M., B. P. Schlitt, and H. L. Lipton.** 2002. Enhanced detection of Theiler's virus RNA copy equivalents in the mouse central nervous system by real-time RT-PCR. J. Virol. Methods **103:**89–99.
51. **Zheng, L., M. A. Calenoff, and M. C. Dal Canto.** 2001. Astrocytes, not microglia, are the main cells responsible for viral persistence in Theiler's murine encephalomyelitis virus infection leading to demyelination. J. Neurovirol. **118:**256–267.